Y. Moreno, A. Egea, G. Almandoz, G. Ugalde, A. Urdangarin and R. Moreno, "High-Frequency Modelling of Windings," 2022 International Conference on Electrical Machines (ICEM), 2022, pp. 1232-1238.

DOI: https://doi.org/10.1109/ICEM51905.2022.9910696

High-Frequency Modelling of Windings

Yerai Moreno, Aritz Egea, Gaizka Almandoz, *Member, IEEE*, Gaizka Ugalde, *Member, IEEE*, Ander Urdangarin and Roberto Moreno

***Abstract*—Electrical drives consume a great amount of the world's energy, and this will keep increasing due to the electromobility trend. Hence, the efficiency of electrical drives must be improved to reach sustainability. Silicon Carbide devices have a high working frequency and lower switching loss, increasing the device efficiency. Nevertheless, higher operation frequencies may bring major Electromagnetic Compatibility issues, in addition to insulation stress and higher bearing currents. This paper presents the simulation process to obtain a high-frequency model of an electrical machine. Then, some small and controlled coils are modelled to construct the high-frequency model step by step, analysing the slight differences between conductor diameters and materials that would be difficult to see in a machine. These models are validated with experimental impedance measurements. This represents the first step in modelling an electrical machine equivalent circuit to predict the electromagnetic interference levels from the design stage.**

***Index Terms*—Coils, Computer simulation, Electromagnetic compatibility, Finite element analysis, High Frequency.**

I. Introduction

In the context of electrifying mobility, it is crucial to improve the efficiency of electrical drives, so that both air pollution and energy consumption are reduced. Silicon Carbide (SiC) devices can play a key role in this objective due to their high working frequency and efficiency. However, working at higher frequencies can cause serious Electromagnetic Interference (EMI) problems, and it can also affect the robustness of electrical machines.

A typical electrical drive consists of three main elements: the energy source (batteries in e-mobility applications), the converter that supplies the desired voltage and frequency to the electrical machine using the Pulse Width Modulation (PWM) technique, and the electrical machine. PWM pulses produce a Common-Mode (CM) voltage in the input connection of the motor causing diverse problems such as shaft voltage and bearing currents [1]. Fast voltage changes (high du/dt) also damage the winding insulation due to overvoltages, and short-circuit or contact defects may cause safety breakdowns [2]. In addition, the resulting EMI can affect the power source grid and all elements connected to it, for example, sensors and safety systems in electric cars [3].

EMI is the degradation of the performance of electrical equipment. There are two main types depending on the propagating medium: conducted and radiated. Conducted EMI flows through wires from the source of interference (the inverter) to a susceptible receiver, which could be a motor or any electrical device connected to the power grid. It covers a frequency range from 150 kHz to 30 MHz. In contrast, radiated EMI propagates through the environment when there is a wire acting as an antenna [4], covering a frequency range from 30 MHz to 100 MHz.

To limit this interference, Electromagnetic Compatibility (EMC) standards have been defined to allow equipment to function satisfactorily in the electromagnetic environment without introducing intolerable electromagnetic disturbances.

A number of approaches have been proposed to comply with the EMC standards in electrical drives. Several types of inverters and modulation techniques were presented in [1], [5], [6] to reduce CM voltages from the inverter. In addition, some filters to prevent EMI from extending to the power grid were proposed in [7]. Then, to reduce the undesired effects of CM voltages– bearing currents or EMI–shieldings, grounding wires and insulated bearings are widely used [5], however, they increase the cost, volume, and weight of the drive.

Therefore, to minimise the development cost of the product and increase its reliability, an EMC approach should be added at the beginning of the machine design methodology. Consequently, understanding and predicting EMI noise using a high-frequency model of an electrical machine during the design stage is essential to manage EMI problems at the device level. DM and CM impedances are used to predict the machine behaviour at different frequencies. From these impedances, the CM and DM currents caused by the converters can be modelled. In [8], an empirical high-frequency electrical drive model was presented. However, to focus on designing electrical machines from the EMC perspective, it is necessary to develop this model by other means, such as Finite Element Method (FEM) simulations. This is because measuring the impedance of the machine is not feasible at the design stage.

Most publications found in the literature deal directly with machine models [9]–[12], without detailing all phenomena that occur in these machines when working at high frequency. Usually, electrical machines are complex devices with a high number of turns per coil and connections between windings and phases. Additionally, at high frequency, a significant

The work of Yerai Moreno was funded in part by the Non-Doctoral Research Staff Training Programme of the Department of Education of the Basque Government through grant PRE-2021-2-0057.

The work of the other authors was funded in part by the Department of Economic Development and Competitiveness of the Basque Government through Elkartek grant KK-2021/00044.

Y. Moreno, A. Egea, G. Almandoz and G. Ugalde are with Mondragon Unibertsitatea, Faculty of engineering, Mondragón, 20500, Gipuzkoa, Spain (e-mail: ymoreno@mondragon.edu, aegea@mondragon.edu, galmandoz@mondragon.edu, gugalde@mondragon.edu)

A. Urdangarin is with ORONA EIC, Hernani, 20120, Gipuzkoa, Spain (e-mail:aurdangarinl@orona-group.com)

R. Moreno is with IKERLAN, Mondragón, 20500, Gipuzkoa, Spain (e-mail: rmoreno@ikerlan.es)

number of parasitic capacitances appear, together with core losses. This makes it difficult to analyse the influence of small changes in the impedance of the motor.

The main contribution of this study, therefore, is a detailed analysis of these high-frequency phenomena using small and controlled coil models. With the conductors uniformly located, the influence of conductor diameters and core materials on the impedance of a coil can be observed. No published work has been found which approaches the analysis in this way. This approach serves as the first step to modelling a full electrical machine at high frequency.

In the present paper, the simulation process for a coil working at high frequency is explained, comparing the behaviour of several core materials. First, high-frequency phenomena are described. Second, the high-frequency modelling process is explained. Finally, the models are validated by experimental impedance measurements in the range of 100 Hz - 100 MHz.

II. Description of High Frequency Phenomena

In low-frequency operations, resistance and inductance values barely change with frequency, and thus can be considered constants. Nevertheless, as frequency increases, some new phenomena emerge, leading to an increase in resistance and a decrease in inductance [13].

The skin effect is one phenomenon that appears as the frequency increases. Eddy currents are induced in the conductor due to the magnetic field. These Eddy currents cause a non-uniform current density inside the conductor, as the electrons are pushed to the perimeter of the conductor. In this way, the effective cross-section of the conductor decreases with frequency, since the current flows only in the skin depth of the conductor. The current density of a conductor is shown in Fig.1 at different frequencies.

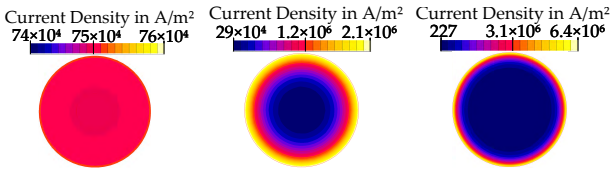

Fig. 1: Skin effect in a conductor of 1.5 mm of diameter. (**a**) 1 kHz. (**b**) 100 kHz. (**c**) 1 MHz.

This surface current distribution increases resistance and decreases inductance due to flux distribution inside the conductor. The skin effect can be defined as independent since it solely depends on frequency and geometry. Thus, it can be analysed by simplifying the problem with a single conductor [14], [15], and can be mitigated by using a smaller conductor diameter than the skin depth.

However, the surrounding conductors of the coil cause another effect called the proximity effect, which is more significant than the skin effect [10]. This concept is similar to the skin effect, but considers the effect of induced Eddy currents in a conductor due to the magnetic field generated by the nearby conductors. Therefore, this phenomenon depends on the geometrical configuration of the coil conductors and can be mitigated using windings with parallel strands or Litz wires. These latter are difficult to manufacture and can generate unbalanced current distribution across the strands [11], and are also counterproductive at very high frequencies. The non-uniform current distribution caused by this effect in an electrical machine coil is shown in Fig.2. The current distribution is not uniform in the slot, or in any individual conductor. When both phenomena occur together, the effective cross-section of the conductor decreases further, resulting in a greater resistance increase [12], [16].

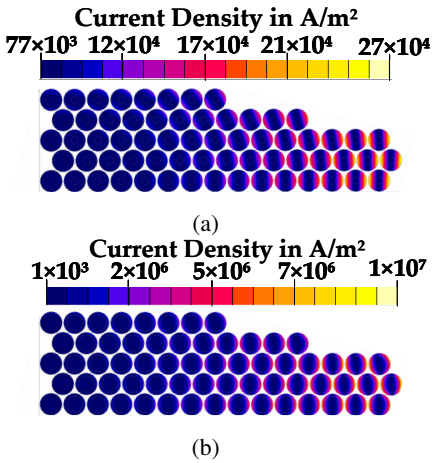

Fig. 2: Proximity effect in a middle slot of a machine. (**a**) 1 kHz (**b**) 100 kHz.

High-frequency phenomena also appear in the magnetic core of electrical machines, which significantly influences the motor impedance behaviour. Typically, both stator and rotor magnetic cores are laminated with electrical steel sheets to limit the Eddy currents induced by alternating magnetic fields, which reduces magnetic losses. Nevertheless, when the skin depth of these sheets becomes thinner than their width, Eddy currents start flowing, increasing magnetic losses. This increase is due to the proximity effect between the laminated sheets. The induced Eddy currents create a shielding effect inside the electrical sheets, pushing the magnetic flux out of the iron core, which causes a decrease in the relative permeability of the magnetic material, and in the inductance value of the coil.

The threshold frequency of this shielding effect depends on the thickness of each steel sheet and its resistivity. It should be noted, however, that the effect of lamination is counterproductive due to the proximity effect between the laminated sheets. Nevertheless, the flux is not completely pushed out of laminated cores, as is the case of non-laminated cores [16].

Finally, the influence of parasitic capacitances must be taken into account. At low frequencies, these are insignificant as their impedance is usually large. However, as the frequency increases, the impedance of the parasitic capacitance

decreases, leading to new current flow paths inside the motor. This has a considerable effect on the differential and common-mode impedances and currents of the machine [12]. The main parasitic capacitances involved in an electrical motor are between parts at different voltages, such as the winding, the stator, the rotor, the bearings, and the shaft.

III. Simulation Process

The general process to obtain a high-frequency model of an electrical machine is summarised in Fig.3.

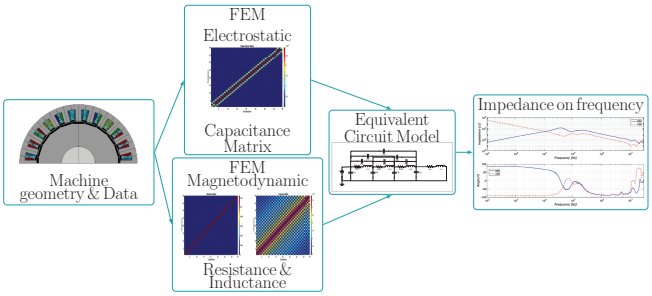

Fig. 3: High-frequency FEM Modelling Process.

First, the geometry and materials of the machine or device to model are defined. Then, two different FEM simulations must be carried out: One to obtain the capacitances that simulate the electrical fields in an electrostatic simulation, and another to calculate the resistance and inductance that simulates the electromagnetic effects in a magneto-dynamic environment.

Next, these RLC parameters must be incorporated into a Lumped Parameter Model (LPM) equivalent circuit that describes the connection between the RLC elements in the device.

Finally, by solving the equivalent circuit, the impedance is obtained for the desired frequency range. Even if the EMC frequency range for conducted emissions is from 150 KHz to 30 MHz, it is advisable to expand the frequency range above and below those limits. In this way, resonances that may appear within that limit are shown properly in the model.

A. Magnetic Finite Element Simulation

The magnetic simulation is performed, resulting in the resistance and inductance values of each turn at different frequencies.

1) Geometry & Mesh: The geometry of the element must be defined. At high frequency, details of the conductors are important, as skin and proximity effects appear in conductive elements, and they affect the resistance and inductance values. Therefore, each winding conductor must be drawn individually, although typically when simulating electrical machines, the entire slot is taken as a single conductor.

Altair Flux was used to model the electrical machine in FEM. Using this software a solid conductor can be modelled in three ways, as shown in Fig.4.

The easiest (Fig.4a), consists of drawing a circle with the conductor diameter and assigning it to a solid conductor.

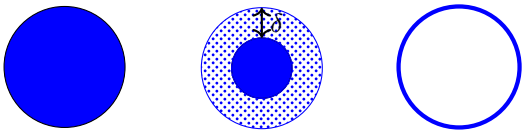

Fig. 4: Conductor Modelling. **(a)** Solid conductor. **(b)** Solid conductor with adaptive meshing. **(c)** Surface Impedance.

This is suitable for low frequencies, when the skin depth is not very pronounced. It is also economical in terms of mesh and solving time.

Going one step further, in Fig.4b, another circle is drawn inside the previous conductor, with a variable diameter set as $D_{in} = D_{cond} - \delta$, where δ is defined as the skin depth of the material. In this way, the mesh is automatically adjusted to the working frequency of the device. The main drawback of this method is the increase in meshing nodes and solving time. If the skin depth is too low, it can also cause meshing errors.

A third option has been recently introduced to the software, called surface impedance. As described in Fig.4c, the conductor is solely defined by the exterior surface. This option is only available for 3-D models because in 3-D the computation time is much higher, and implementing a variable mesh can be unfeasible. With this option, as the interior of the conductor is not meshed, the solving time is reduced significantly, but the result is only valid for very high frequencies.

In summary, the only way to model the conductor properly for the whole frequency range is by using the solid conductor with adaptive mesh.

2) Simulation Type & Domain: To define the domain, an air box is established, which must be big enough for the flux lines of the device to be calculated. Then, the type of simulation is determined. For the present simulations, as there were no magnets, magnetic and electrical variables were considered sinusoidal, and thus steady-state simulation was used, by performing a frequency sweep. However, time-dependent transient simulation must be used when magnets are introduced because the magnetic field they produce is not sinusoidal. For instance, magnets are needed when modelling the rotor of a permanent magnet synchronous electrical machine.

Usually, resistance and inductance results are sufficiently accurate with 2-D simulations, but if the end-windings are proportionally longer than the active part, 3-D simulations may be used. They may also be employed to consider the lamination effect of ferromagnetic sheets.

3) Material Characterisation: Copper is mainly used for winding turns. It is easily defined by its resistivity and unitary permeability. Each conductor must be linked to a solid conductor in a circuit. The direction of the current must also be assigned, as shown in Fig.7b.

Ferromagnetic materials are used for the stator and rotor. As they are non-linear, characterisation is carried out with the BH curve, together with its resistivity. It is important to note

that the amplitude of high-frequency excitation signals is normally very low compared to those at operation frequencies, so the material will remain in the lower part of the BH curve. As for conductors, a solid conductor must also be linked to the core, so that the induced Eddy currents are calculated.

B. Electric Finite Element Simulation

When two electrical components or circuits at different voltages are close to each other, charge storage happens due to the electric field. This unavoidable effect is called parasitic capacitance, and it is present in all practical circuit elements such as inductors, diodes, coils, and of course, in electrical machines. This is a significant problem in high-frequency circuits and is often the factor limiting the operating frequency and bandwidth of electronic components.

The same geometry employed for inductance calculation is used for capacitance calculation. However, as the electric fields must be analysed, the FEM software application has to be changed to electrostatic, and the faces and materials must be re-defined with electrical characteristics. Drawing the insulating parts is essential in electrostatic simulation, and adaptive meshing is not needed. Nevertheless, a fine mesh is recommended between conductors to obtain accurate results.

Regarding the domain, the limits of the simulation must be defined by setting an infinite box, which rounds the simulated elements. This region is defined as air and it is the boundary condition.

There are three types of regions:

- **Perfect conductor:** Conductive elements, such as the conductors themselves, the core of a coil or the stator of a machine must be defined as perfect conductors as their surfaces are assumed to be equipotential.
- **Dielectric region:** Impregnation and insulation elements must be defined as dielectric so that the permittivity can be defined. For example, the insulating paper Nomex 410 used in the slots has a dielectric constant of 2.9.
- **Line region:** The surface of the conductive elements must be set to 0 or 1 V potential to obtain the capacitance matrix. This is because the surface of the conductor is considered equipotential.

Once all the regions are defined, the process to obtain the capacitance matrix is the following: A 0 V voltage is assigned to all conductors in their line regions. Then, in each of the N simulations, the i conductor is set to 1 V and the electric field distribution is solved.

Finally, with $C_{ij} = 2\frac{Q_{ij}}{V_j}$ the desired capacitances are obtained and included in the matrix, where the Q_{ij} is the electric charge and V_j is the applied voltage. After the N simulations, a full NxN matrix is obtained using the capacitances between the conductors.

The diagonal parameters are the self-capacitances that usually do not have a practical meaning for the defined circuit. The useful capacitances are the off-diagonal ones, representing the capacitances from conductor i to j and vice versa because the matrices are symmetric.

C. Distributed Parameter High-Frequency Model

The model presented in [17] is used, as it takes into account the inter-turn capacitances of the coils, which are important to model the high-frequency resonances. Its main advantage is the matrix form, which facilitates its ease of use and efficiency. The lumped parameter circuit can be seen in Fig.5. It is valid for n turns, but just 4 turns are illustrated due to space constraints. This equivalent circuit is solved using *Matlab* software.

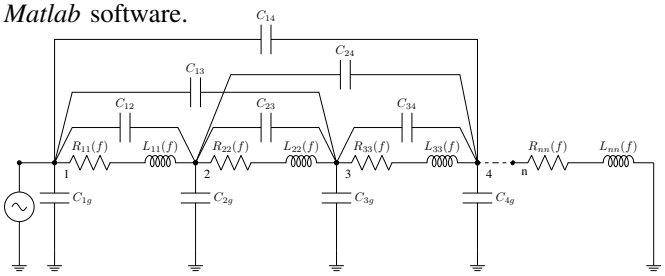

Fig. 5: Used Equivalent Circuit.

Kirchhoff's voltage and current laws can be used to solve the n nodes in Fig.5, and the following matrix equation is obtained:

$$\left(j\omega \begin{bmatrix} L(\omega) & 0 \\ 0 & C \end{bmatrix} - \begin{bmatrix} R(\omega) & D \\ -D^T & 0 \end{bmatrix}\right) \begin{Bmatrix} \{I\} \\ \{U\} \end{Bmatrix} = \begin{Bmatrix} \{b_1\} \\ \{b_2\} \end{Bmatrix} \quad (1)$$

It should be noted that the L and R matrices are frequency dependent, whereas the capacitance matrix is constant over frequency. D matrix is defining the circuit. Vectors $\{b_1\} = \{V_1, 0, \ldots, 0\}$ and $\{b_2\} = j\omega U_1 C_{2,1}, C_{3,1}, \ldots, C_{n,1}$ can be considered source terms for solving. In this case, as the Differential-mode of a coil was calculated, the terms $C_{i,g}$ refer to $C_{i,n}$, but they can be used as turn-to-core capacitance on Common-mode measurements.

IV. Experimental Validation

The Omicron Bode100 was used from 50 Hz to 50 MHz with the series-thru layout shown in Fig.6, while the Siglent SSA3032X-R covered the 5 to 100 MHz range with the same layout.

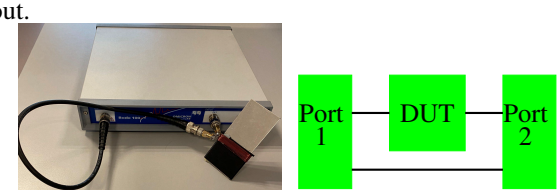

(a) (b)

Fig. 6: Experimental validation. (**a**) Test rig. (**b**) Layout.

V. Case Studies

An ABS plastic reel was pierced to introduce different material sheets. Initially, an ABS sheet was introduced to validate the model. Then, aluminium and M800-65A sheets were inserted, including Eddy currents and magnetic effects respectively.

The FEM model is shown in Fig.7a, together with the coupled circuit for the magnetic simulation in Fig.7b.

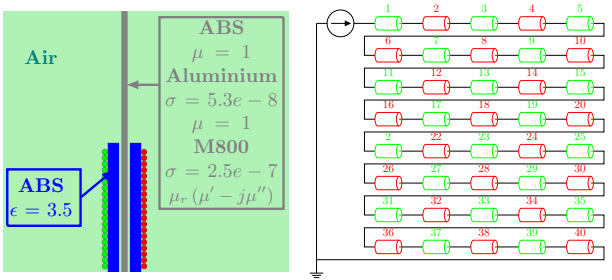

(a) (b)

Fig. 7: FEM Model C. **(a)** Geometry & Materials. **(b)** Circuit.

The same model was used for the three sheet materials, the only difference was the resistivity (σ) and permeability (μ) values of the materials of the sheets. Moreover, for the aluminium and M800-65A sheets, an extra solid conductor was defined to consider the Eddy currents.

Then, for the electrostatic simulation, the same geometry was used, defining the ABS dielectric, and the impregnation of the conductors. The sheet was defined as a conductor.

A. *ABS cored coil*

From the magnetic simulation, the resistance and inductance curves were obtained, as illustrated in Fig.10. Regarding the electrostatic simulation, the same geometry was used, by defining the ABS dielectric, and the impregnation of the conductors. The capacitance matrix of the ABS sheet coil is depicted in Fig.8. As in the other analysed cases, the biggest capacitances are those with adjacent turns, and they keep decreasing with distance. In the ABS case for example, $C_{5,6} = 8.3E-15$.

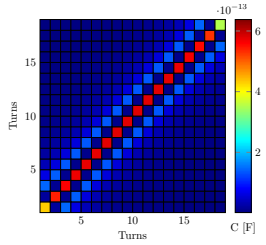

Fig. 8: Capacitance matrix of ABS cored coil.

Next, the model was compared with the measurement in Fig.9. Two conductor diameters were modelled. Both models showed good agreement with the measurements in the whole range. the resonance point in the models was a bit lower than the measurement, but this may be due to material or geometrical tolerances. It can be seen that the higher the diameter of the conductor, the lower the impedance and the higher the resonance frequency.

Since the resonance point was above 50 MHz, it was necessary to measure with two different measuring devices. The Omicron Bode100 was used from 50 Hz to 50 MHz, while the Siglent SSA3032X-R covered the 5 to 100 MHz range. It can be seen that both devices measure the same impedance value from 5 to 50 MHz, but not the phase value. This is not significant, as the resonance point is identified in both the impedance and phase values, but it causes a gap in the phase value between the two measures at 50 MHz.

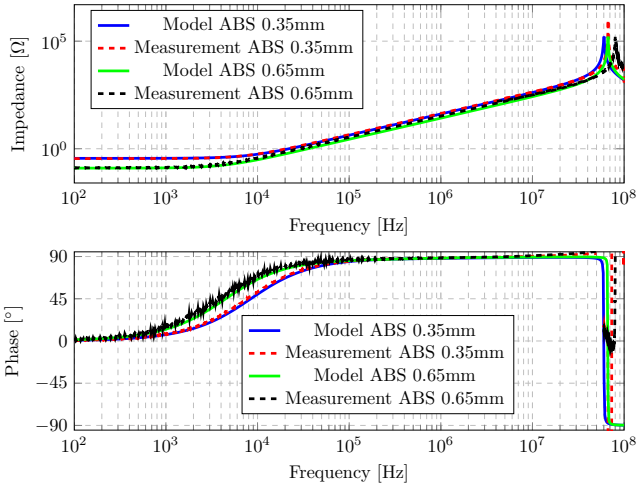

Fig. 9: Validation of model with ABS sheet.

B. *Aluminium cored coil*

In Fig.10 a comparison is made between the aluminium and ABS sheet resistance and inductance values.

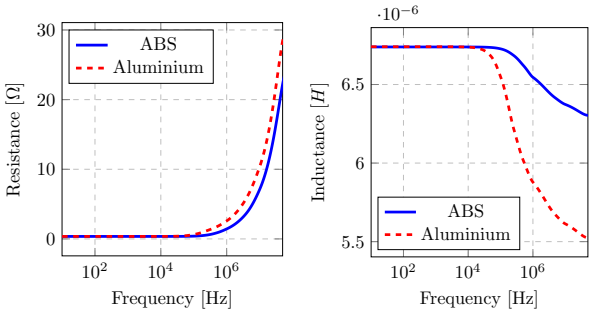

(a) (b)

Fig. 10: FEM Model. Comparison between ABS and Aluminium sheet. **(a)** Resistance. **(b)** Inductance.

It can be seen that at low frequency (until 10^5 Hz), resistance and inductance values are equal for both sheets, as the permeability of aluminium is similar to vacuum. However, when the frequency increases, the resistance of the aluminium sheet coil increases further, whereas the inductance decreases with respect to the ABS sheet coil.

This is due to Eddy currents in the aluminium sheet. On the one hand, they increase the loss of the coil due to the Joule loss, increasing the resistance. On the other hand, the Eddy currents in the aluminium sheet cause a shielding effect to the magnetic flux generated by the coil, preventing the flux from going through the sheet, decreasing the inductance. In Fig.11, this effect can be appreciated.

In Fig.11a the magnetic field can be seen at 100 Hz, where it goes through the aluminium sheet, whereas in Fig.11b the shielding effect appears and the flux is stopped outside the sheet. This is the cause of the more pronounced inductance decrease in the aluminium sheet. In this case, the capacitance

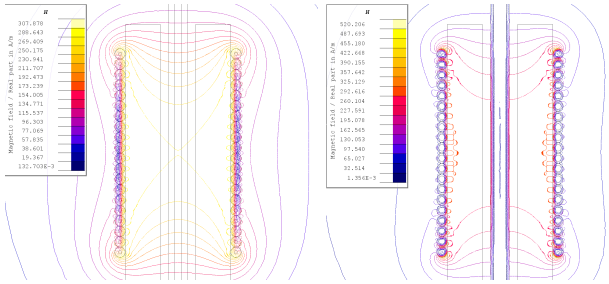

(a) (b)

Fig. 11: Aluminium sheet. Shielding effect. **(a)** H at 100 Hz. **(b)** H at 1 MHz.

$C_{5,6}$ is $4.5E-15$, nearly half of the ABS coil, due to the conductive sheet inside the reel.

As concluded from Fig.12, the model shows good agreement with the measurement in the whole range too. There is a small resonance point in the measurement next to the principal resonance point that is not observed in the model.

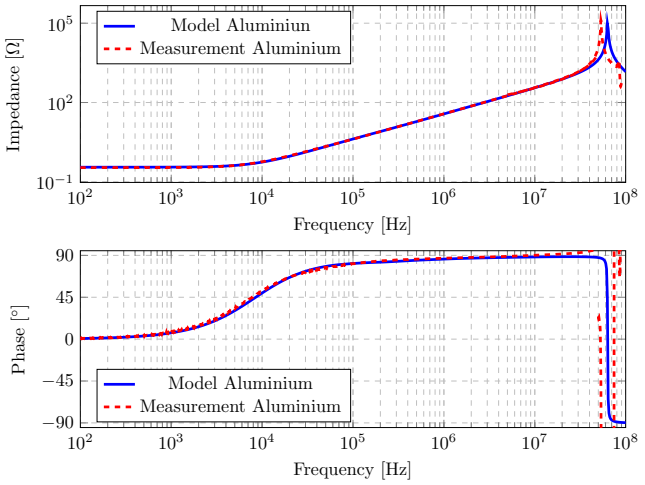

Fig. 12: Validation of the model with aluminium sheet.

C. Ferromagnetic cored coil

A sample of an electrical sheet was selected to analyse its behaviour at high frequency. 20 turns were given to the reel with the M800 sheet. The comparison of the resistance and inductance values of the ABS and M800 sheets are shown in Fig.13.

In this case, the resistance is equal at lower frequencies, but it increases for the M800 sheet at high frequencies. This effect is due to the Eddy currents in the sheet. It increases further than in the aluminium case because the resistivity of the M800 is higher, so more losses are produced.

Moreover, the inductance is higher in the M800 sheet at low frequency, as the M800 has higher permeability than air. However, as the frequency rises, the inductance becomes equal to the ABS case, and even lower, since the shielding effect of the sheet caused by the Eddy currents prevents the flux from passing through it. Fig.14 shows the impedance of the model with the M800 sheet. It shows a good matching

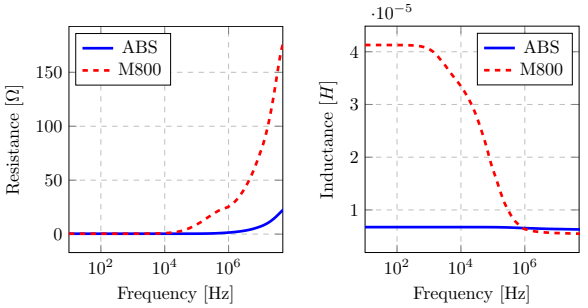

(a) (b)

Fig. 13: FEM Model. Comparison between ABS and M800 sheet. **(a)** Resistance. **(b)** Inductance.

with the measurement with minor differences in the phase, that may be due to the magnetic properties of the material.

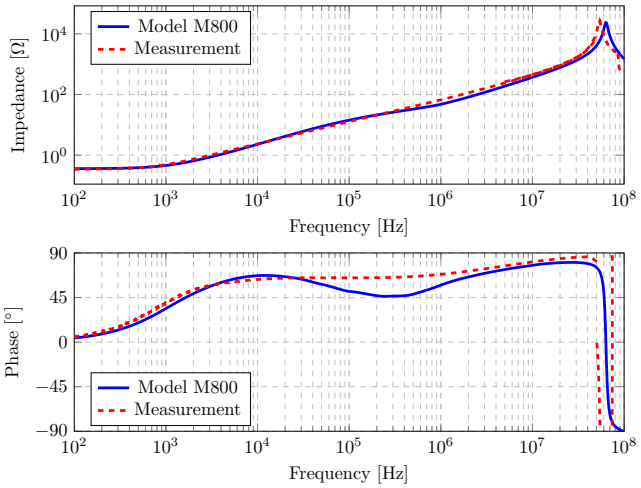

Fig. 14: Validation of model with M800 sheet.

VI. Conclusions

The modelling of electrical machines at high frequency is complex, as different characteristics influence the result. These characteristics are multi-physic, requiring diverse simulations to obtain the parameters. Thus, in this paper simple and controlled models were used to simulate the high-frequency phenomena that are difficult to analyse in a full electrical machine, and the following conclusions were drawn:

The quality of the mesh on the conductor surface must be fine to consider the skin and proximity effects in FEM simulations. This effect is emphasised in 3-D, where developing a thinner mesh can significantly increase simulation time and computing requirements. Thus, 2-D models are preferred if the end-windings are small in proportion to the full coil.

The proposed models were validated, and it was found that the defined FEM simulation process and the employed LPM are valid and accurate, including resistance, inductance, and capacitance values.

The models were able to simulate the influence of core materials, together with different conductor diameters. Both

the aluminium and the M800 showed good agreement with the measured impedance.

The models presented in this paper serve as the first step toward modelling electrical machines at high frequency. In fact, electrical machines consist of a number of coils in series in each phase. Thus, once the FEM tool is calibrated and validated with small coils, a coil with a higher number of turns divided into more than one layer must be validated, as machine coils are usually multi-layer.

Then, the used equivalent circuit can be extended to the necessary coils for each phase. Finally, the DM model of an electrical machine will be obtained by connecting the three phases with their capacitive couplings. In addition, by linking the capacitive couplings from the winding to the stator, and connecting the equivalent circuit properly, the CM model can also be achieved.

It must be noted that the calculation effort for the analysed coils is small, but it will increase for a higher number of coils in the machine. Thus, an equilibrium between accuracy and computation effort is needed.

REFERENCES

[1] J. Zhang, M. Shen, and X. Zhao, "Study on the Effect of Inverter Modulation Methods and Operating Condition on Common Mode EMI for Motor Drive System," in *SAE Technical Papers*, vol. 2017-March, no. March, 3 2017. [Online]. Available: https://www.sae.org/content/2017-01-1223/

[2] Z. Shen, D. Jiang, T. Zou, and R. Qu, "Dual-Segment Three-Phase PMSM With Dual Inverters for Leakage Current and Common-Mode EMI Reduction," *IEEE Transactions on Power Electronics*, vol. 34, no. 6, pp. 5606–5619, 6 2019. [Online]. Available: https://ieeexplore.ieee.org/document/8440757/

[3] G. Spadacini, F. Grassi, and S. A. Pignari, "Conducted emissions in the powertrain of electric vehicles," *IEEE International Symposium on Electromagnetic Compatibility*, vol. 69, no. July, pp. 1–15, 2017.

[4] L. Dawson, A. Rowell, R. Armstrong, and A. Ruddle, "EMC Design Guidelines for manufacturers of vehicle electric drives," York EMC Services, York, Tech. Rep. 314609, 2014. [Online]. Available: https://www.researchgate.net/publication/335724266_EMC_Design_Guidelines_for_manufacturers_of_vehicle_electric_drives_HEMIS_Deliverable_61

[5] E. Robles, M. Fernandez, E. Ibarra, J. Andreu, and I. Kortabarria, "Mitigation of common mode voltage issues in electric vehicle drive systems by means of an alternative AC-decoupling power converter topology," *Energies*, vol. 12, no. 17, p. 3349, 8 2019. [Online]. Available: https://www.mdpi.com/1996-1073/12/17/3349

[6] K. Vostrov, J. Pyrhonen, M. Niemela, J. Ahola, and P. Lindh, "Mitigating noncirculating bearing currents by a correct stator magnetic circuit and winding design," *IEEE Transactions on Industrial Electronics*, vol. 68, no. 5, pp. 3805–3812, may 2021. [Online]. Available: https://ieeexplore.ieee.org/document/9057574/

[7] T. Weber, "EMC filters in high voltage traction drive systems," *IEEE International Symposium on Electromagnetic Compatibility*, 2008.

[8] G. Almandoz, S. Zarate, A. Egea, Y. Moreno, A. Urdangarin, and R. Moreno, "High Frequency Modeling of Electric Drives for Electromagnetic Compatibility Analysis," in *2020 International Conference on Electrical Machines (ICEM)*. IEEE, 8 2020, pp. 1129–1135. [Online]. Available: https://ieeexplore.ieee.org/document/9270804/

[9] J. E. Ruiz-Sarrio, F. Chauvicourt, J. Gyselinck, and C. Martis, "High-frequency modelling of electrical machine windings using numerical methods," in *2021 IEEE International Electric Machines & Drives Conference (IEMDC)*. IEEE, 05 2021, pp. 1–7. [Online]. Available: https://ieeexplore.ieee.org/document/9449561/

[10] O. Mohammed, S. Ganu, N. Abed, S. Liu, and Z. Liu, "High frequency PM synchronous motor model determined by FE analysis," *IEEE Transactions on Magnetics*, vol. 42, no. 4, pp. 1291–1294, 4 2006. [Online]. Available: http://ieeexplore.ieee.org/document/1608450/

[11] A. Al-Timimy, P. Giangrande, M. Degano, M. Galea, and C. Gerada, "Investigation of AC Copper and Iron Losses in High-Speed High-Power Density PMSM," in *2018 XIII International Conference on Electrical Machines (ICEM)*. IEEE, 9 2018, pp. 263–269. [Online]. Available: https://ieeexplore.ieee.org/document/8507166/

[12] B. Heidler, K. Brune, and M. Doppelbauer, "High-frequency model and parameter identification of electrical machines using numerical simulations," in *2015 IEEE International Electric Machines & Drives Conference (IEMDC)*. IEEE, 5 2015, pp. 1221–1227. [Online]. Available: http://ieeexplore.ieee.org/document/7409217/

[13] Y. Moreno, G. Almandoz, A. Egea, B. Arribas, and A. Urdangarin, "Analysis of Permanent Magnet Motors in High Frequency—A Review," *Applied Sciences*, vol. 11, no. 14, p. 6334, jul 2021. [Online]. Available: https://www.mdpi.com/2076-3417/11/14/6334

[14] S. Kim and D. P. Neikirk, "Compact equivalent circuit model for the skin effect," *IEEE MTT-S International Microwave Symposium Digest*, vol. 3, pp. 1815–1818, 1996.

[15] N. Idir, Y. Weens, and J. J. Franchaud, "Skin effect and dielectric loss models of power cables," *IEEE Transactions on Dielectrics and Electrical Insulation*, vol. 16, no. 1, pp. 147–154, 2009.

[16] Kohji Maki, Hiroki Funato, and Liang Shao, "Motor modeling for EMC simulation by 3-D electromagnetic field analysis," in *2009 IEEE International Electric Machines and Drives Conference*. IEEE, 5 2009, pp. 103–108. [Online]. Available: http://ieeexplore.ieee.org/document/5075190/

[17] P. Brauer, "High-Frequency Voltage Distribution Modelling of a Slotless PMSM from a Machine Design Perspective," 2018.

VII. BIOGRAPHIES

Yerai Moreno was born in Irún, Spain, in 1996. He received the B.Sc. degree in electrical engineering from the University of the Basque Country, Spain in 2018 and the M.S. degree in industrial engineering from Mondragon Unibertsitatea, Spain, in 2020. Since 2018, he has been with the Electronics and Computing Department, Mondragon Unibertsitatea, where he is currently pursuing his PhD. His current research interest includes permanent magnet machine design and EMC optimisation of electrical drives.

Aritz Egea received the degree in electrical engineering from the University of Mondragon, Mondragón, Spain, in 2009, and the PhD degree in electrical engineering in 2012. He is currently an Associate Professor at the Faculty of Engineering, Mondragon Unibertsitatea. His current research interests include electrical machine design and control and electromagnetic actuators.

Gaizka Almandoz (M'04) was born in Arantza, Spain. He received the B.Sc. and PhD degrees in electrical engineering from Mondragon Unibertsitatea, Mondragón, Spain, in 2003 and 2008, respectively. Since 2003, he has been with the Electronics and Computing Department, Mondragon Unibertsitatea, where he is currently an Associate Professor. His current research interest includes electrical machine design, modelling, and control. He has participated in various research projects in the fields of wind energy systems, elevator drive, and railway traction.

Gaizka Ugalde (M'07) received the B.Eng. and PhD degrees in electrical engineering from Mondragon Unibertsitatea, Mondragón, Spain, in 2006 and 2009, respectively. Since 2009, he has been with the Department of Electronics, Mondragon Unibertsitatea, where he is currently an Associate Professor. His current research interest includes permanent-magnet machine design, modelling, and control. He has participated in various research projects in the fields of renewable energy and people transportation systems.

Ander Urdangarin was born in Ordizia. Spain, in February 1982. He received the B.Sc. degree in Automatic and industrial electronics from Mondragon Unibertsitatea, Mondragón, Spain, in 2009. Between 2010-2012, he was with the Department of Electronics of Mondragon Unibertsitatea. Since 2012, he is a member of ORONA. His current research interests include power electronics design, modelling, and control.

Roberto Moreno was born in Eibar, Spain, in May 1974. He received the B.S. degree in electronic engineering from Mondragon Unibertsitatea, Mondragón, Spain, in 1998. Since 1998, he has been with the Department of Electronics (now Hardware Systems and Comunications Area), in Ikerlan Research Center. Since 2008, he is the head of EMC and non-functional requirements laboratory and researcher. His current research interests include electrical and electronic behaviour analysis and simulation of power and control electronics in the EMC area.